Linearization of a Naturally Occurring Circular Protein Maintains Structure but Eliminates Hemolytic Activity[†,‡]

Daniel G. Barry, Norelle L. Daly, Richard J. Clark, Lillian Sando, and David J. Craik*

Institute for Molecular Bioscience, Australian Research Council Special Research Centre for Functional and Applied Genomics, University of Queensland, Brisbane 4072, Australia

Received December 9, 2002; Revised Manuscript Received April 7, 2003

ABSTRACT: Cyclotides are a recently discovered family of disulfide rich proteins from plants that contain a circular protein backbone. They are exceptionally stable, as exemplified by their use in native medicine of the prototypic cyclotide kalata B1. The peptide retains uterotonic activity after the plant from which it is derived is boiled to make a medicinal tea. The circular backbone is thought to be in part responsible for the stability of the cyclotides, and to investigate its role in determining structure and biological activity, an acyclic derivative, des-(24−28)-kalata B1, was chemically synthesized and purified. This derivative has five residues removed from the 29-amino acid circular backbone of kalata B1 in a loop region corresponding to a processing site in the biosynthetic precursor protein. Two-dimensional NMR spectra of the peptide were recorded, assigned, and used to identify a series of distance, angle, and hydrogen bonding restraints. These were in turn used to determine a representative family of solution structures. Of particular interest was a determination of the structural similarities and differences between des-(24−28)-kalata B1 and native kalata B1. Although the overall three-dimensional fold remains very similar to that of the native circular protein, removal of residues 24−28 of kalata B1 causes disruption of some structural features that are important to the overall stability. Furthermore, loss of hemolytic activity is associated with backbone truncation and linearization.

The cyclotides (*1*) are a recently discovered family of small plant-derived circular proteins that have a range of exciting applications in drug design (*2*) and agriculture (*3*). They are typically ∼30 amino acids in size, contain a head-to-tail cyclized backbone, and incorporate three disulfide bonds arranged in a cystine knot motif. In this motif, an embedded ring in the structure formed by two disulfide bonds and their connecting backbone segments is penetrated by the third disulfide bond. The combination of a cystine knot with a circular backbone defines the cyclic cystine knot (CCK)[1] motif. The strong cross-bracing and tight globular fold associated with this motif renders the cyclotides impervious to enzymatic breakdown and makes them exceptionally stable (*4*).

The cyclotides are the largest family of a growing number of circular proteins discovered over recent years in organisms ranging from bacteria to plants to animals (*5*). There is great diversity among the structures of these naturally occurring circular proteins, which include examples both with and without disulfide bonds, but their common feature is a protein backbone comprising a continuous cycle of peptide bonds. So far, little is known about the processing mechanisms that produce such circular proteins, but the cyclic backbone potentially confers advantages over conventional linear proteins, including greater stability and resistance to proteolytic digestion; since circular proteins have no termini, they are resistant to cleavage by exopeptidases. With increasing number of discoveries of naturally occurring circular proteins (*5*) and the design of synthetic variants (*6*−*8*), determining the influence of cyclization on structure and activity has attracted much interest.

This study focuses on the cyclotide family of disulfide rich circular proteins, with the aim of delineating the role of the circular backbone in determining three-dimensional structure and biological activity. A diverse range of biological activities has been demonstrated in cyclotides, including insecticidal (*3*), anti-HIV (*9*), antimicrobial (10), anti-neurotensin (11), cytotoxic (12), and hemolytic (*13*) properties. On the basis of various toxic functions of the cyclotides, it has been suggested that they are likely present in plants for defense purposes (*1*). However, structure−activity relationships have yet to be established for this interesting family of macrocyclic peptides. Many of the bioactivities of the cyclotides can be rationalized on the basis of membrane interactions, so their hemolytic properties provide a useful marker that is conveniently measured. Indeed, hemolytic activity was one of the first bioassays used in the discovery of cyclotides (*13*).

In an earlier study of the prototypic cyclotide kalata B1 (*14*), we found that acyclic permutants in which the peptide

[†] This work was supported in part by a grant from the Australian Research Council (D.J.C.). D.J.C. is an Australian Research Council Senior Fellow.

[‡] The coordinates for des-(24−28)-kalata B1 have been deposited in the Protein Data Bank as entry 1ORX.

* To whom correspondence should be addressed: Institute for Molecular Bioscience, University of Queensland, Brisbane, Australia. Phone: +61 7 3365 4945. Fax: +61 7 3365 1990. E-mail: d.craik@imb.uq.edu.au.

[1] Abbreviations: CCK, cyclic cystine knot; TOCSY, 2D total correlation spectroscopy; NOE, nuclear Overhauser effect; NOESY, NOE spectroscopy; DQF-COSY, double-quantum-filtered correlation spectroscopy; ECOSY, exclusive correlation spectroscopy; WATERGATE, water suppression by gradient-tailored excitation; rmsd, root-mean-square deviation.

10.1021/bi027323n CCC: $25.00
Published on Web 05/16/2003

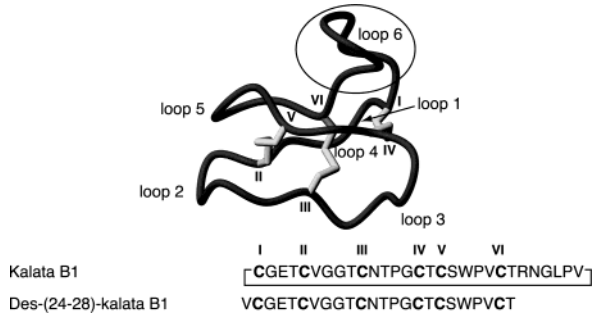

FIGURE 1: Amino acid sequences of kalata B1 and its truncated acyclic permutant des-(24−28)-kalata B1. The six conserved Cys residues are numbered with Roman numerals. The three-dimensional structure of kalata B1 is illustrated above the sequences to show the cyclic cystine knot motif. Loop 6, which is truncated in the permutant, is circled.

cycle was broken in any of the six loops between successive Cys residues in the backbone lost the hemolytic activity that was present in the cyclic parent molecule. However, an analysis of NMR chemical shifts of these permutants showed them to be similar to those in kalata B1, apart from residues near the introduced break in the backbone. The similarity in chemical shifts suggests that the acyclic permutants maintain a three-dimensional fold similar to that of the native structure, but this seemed surprising since biological activity was lost. Since chemical shifts provide only an indirect measure of structure, it was important to undertake a full structural analysis of the acyclic permutants. In this paper, we focus on one of the acyclic mutants, des-(24−28)-kalata B1, in which the backbone segment corresponding to loop 6 of the circular peptide backbone is removed. This loop corresponds to the region of the peptide chain that is involved in the ligation of the termini of a linear precursor protein in the biosynthetic process in plants (*3*). So far, nothing is known of the mechanistic details of the cyclization process, and studies of this acyclic permutant thus have the potential to provide an insight into structural factors that are important in biosynthesis.

Figure 1 shows the generic CCK framework and the sequences of kalata B1 and des-(24−28)-kalata B1. As well as being important as a model for the biosynthetic pathway, this acyclic permutant is topologically equivalent to a range of other linear cystine knot proteins, including those from plants and from animal venoms such as cone snail and spider toxins (*15*). It was therefore of much interest to determine the three-dimensional structure of des-(24−28)-kalata B1 so that it could be compared not only with the native cyclic peptide but also with naturally occurring cystine knot proteins. This study is the first report on the structure of a linearized cyclotide derivative. It has been suggested that the rigid nature of the cyclotide framework makes it useful as a scaffold in drug design (*2*), so determining the role of the cyclic backbone in stabilizing the structure was of interest.

EXPERIMENTAL PROCEDURES

Synthesis and Isolation. Des-(24−28)-kalata B1 was synthesized using solid phase methods as described previously (*14*). Briefly, des-(24−28)-kalata B1 was assembled using manual solid phase peptide synthesis with Boc chemistry. Two forms of the peptide were synthesized, one with a C-terminal amide and the other with a C-terminal carboxylic acid. To produce the C-terminal amide, an MBHA resin was used, whereas the C-terminal acid was generated by attaching the C-terminal threonine to the resin via a PAM linker (Applied Biosystems, Foster City, CA). Amino acids were added to the resin using HBTU with *in situ* neutralization. Cleavage of the peptides from the resin was achieved using hydrogen fluoride with *p*-cresol and *p*-thiocresol as scavengers [9:0.5:0.5 (v/v) HF/cresol/thiocresol mixture]. The crude reduced peptides were purified on a Phenomenex C_{18} column. Gradients of 0.05% aqueous TFA to 90% acetonitrile and 0.045% TFA were employed with a flow rate of 8 mL/min, and the eluent was monitored at 230 nm. These conditions were used in subsequent purification steps.

Oxidation of reduced peptides was achieved by dissolving them in a 50:50 (v/v) 0.1 M NH_4HCO_3 (pH 8.5)/*i*PrOH (0.5 mg/mL) mixture with reduced glutathione added (final concentration of 1 mM). The mixture was stirred at room temperature for 24 h and then purified by RP-HPLC. Identical HPLC profiles were observed for the C-terminal amidated and acid forms. Correctly folded des-(24−28)-kalata B1 was identified by its late eluting time under reverse phase conditions, and ^{1}H NMR spectra confirmed the folded state.

The peptide containing the C-terminal amide was used in the structure determination. This form was previously assayed for hemolytic activity (*14*), and in the current study, the hemolytic activity of the peptide containing the C-terminal acid was assessed. Unless stated otherwise, des-(24−28)-kalata B1 refers to the amidated form in the following discussion.

Native kalata B1 was isolated from *Oldenlandia affinis*. Fresh plant material (150 g) was ground and extracted with a 50:50 (v/v) DCM/MeOH mixture, and the crude extract was partially purified by RP flash chromatography, yielding a fraction containing predominantly cyclotides (1.5 g). This sample was purified further by preparative RP-HPLC to yield pure kalata B1 (98 mg).

Hemolytic Activity Assay. Peptides were dissolved in DMSO and serially diluted in phosphate-buffered saline (PBS) to give 20 μL test solutions in a 96-well U-bottomed microtiter plate (Nunc). Human type A red blood cells (RBCs) were washed with PBS and centrifuged at 4000 rpm for 30 s in a microcentrifuge several times until a clear supernatant was obtained. A 0.25% suspension of washed RBCs in PBS was added (100 μL) to the peptide solutions. The plate was incubated at room temperature for 1 h and centrifuged at 150*g* for 5 min. Aliquots of 100 μL were transferred to a 96-well flat-bottomed microtiter plate (Falcon), and the absorbance was measured at 405 nm with an automatic Multiskan *Ascent* plate reader (Labsystems). The level of hemolysis was calculated as the percentage of maximum lysis (1% Triton X-100 control) after adjusting for minimum lysis [buffer (PBS) control]. Synthetic melittin (Sigma) was used for comparison. The hemolytic dose necessary to lyse 50% of the RBCs (HD_{50}) was calculated using the regression constant from the linear portion of the hemolytic titration curve (Graphpad Prism software).

NMR Spectroscopy. Samples for NMR spectroscopy were prepared by dissolving des-(24−28)-kalata B1 in either a 90% H_2O/10% ^2H_2O mixture or 100% ^2H_2O to a final concentration of 5 mM at pH 4. All spectra were recorded on Bruker ARX 500 and Bruker DMX 750 spectrometers with sample temperatures in the range of 280−330 K. All spectra were acquired in phase sensitive mode using TPPI

(*16*). For resonance assignment and structure determination, a set of two-dimensional (2D) spectra, including DQF-COSY (*17*), TOCSY (*18*) with MLEV17 (*19*) with an isotropic mixing time of 80 ms, ECOSY (*20*), and NOESY (*21*) with mixing times of 100, 150, and 200 ms, were recorded. The water signal in the DQF-COSY spectrum was suppressed by low-power irradiation during the relaxation delay. For the TOCSY and NOESY spectra, water suppression was achieved using a modified WATERGATE (*22*) sequence. All 2D spectra were collected over 4096 data points in the f_2 dimension and 512 or 600 increments in the f_1 dimension and processed using XWINNMR (Bruker). The f_1 dimension was generally zero-filled to 2048 real data points with the f_1 and f_2-dimensions being multiplied by a sine-squared function shifted by 90° prior to Fourier transformation. Spectra were internally referenced to DSS.

Structure Calculations. For des-(24−28)-kalata B1, interproton distance restraints were derived from cross-peaks in NOESY spectra recorded with a mixing time of 200 ms. The cross-peaks were analyzed and integrated within the program XEASY (*23*) and structures calculated within the DYANA package (*24*). After an iterative process where preliminary structures were used to resolve ambiguities, a set of 297 interresidue distance restraints, including 123 sequential, 64 medium-range, and 110 long-range restraints, was derived for des-(24−28)-kalata B1. In addition, the spectral data allowed the introduction of 14 backbone dihedral angle restraints based on $^3J_{HNH\alpha}$ coupling constants derived from the splitting of the amide signals in the one-dimensional (1D) spectra and 11 χ_1 dihedral angles based on $^3J_{H\alpha H\beta}$ coupling constants derived from ECOSY spectra together with NOE intensities derived from a 100 ms NOESY spectrum. Finally, after analysis of preliminary structures and amide exchange data, 10 restraints for five hydrogen bonds were added. After initial structure calculations using DYANA (*24*), sets of 50 structures were calculated using a torsion angle simulated annealing protocol within CNS (*25*). This protocol involves a high-temperature phase comprising 4000 steps of 0.015 ps of torsion angle dynamics, a cooling phase with 4000 steps of 0.015 ps of torsion angle dynamics during which the temperature is lowered to 0 K, and finally an energy minimization phase comprising 500 steps of Powell minimization. The resultant structures were subjected to further molecular dynamics and energy minimization in a water shell (*26*). The refinement in explicit water involves the following steps: (1) heating to 500 K via steps of 100 K, each comprising 50 steps of 0.005 ps of Cartesian dynamics; (2) 2500 steps of 0.005 ps of Cartesian dynamics at 500 K before a cooling phase where the temperature is lowered in steps of 100 K, each comprising 2500 steps of 0.005 ps of Cartesian dynamics; and (3) minimization of the structures with 2000 steps of Powell minimization. Structures were analyzed using PROMOTIF (*27*) and PROCHECK-NMR (*28*).

RESULTS

Des-(24−28)-kalata B1 was synthesized using solid phase chemistry and oxidized in a buffer containing ammonium bicarbonate in 50% aqueous 2-propanol (v/v) to form the three disulfide bonds. HPLC was used to separate the native disulfide isomer from misfolded products, with the native isomer having a characteristic late elution time, as illustrated in Figure 2. The correct disulfide connectivity was subsequently confirmed from NMR experiments. NMR spectra were recorded at 500 and 750 MHz and used to determine the three-dimensional structure of the peptide.

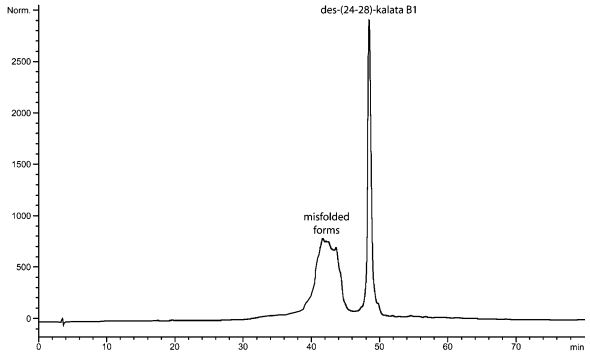

FIGURE 2: Reverse phase HPLC for the oxidation reaction of des-(24−28)-kalata B1 clearly distinguishing the correctly folded des-(24−28)-kalata B1 from the misfolded species.

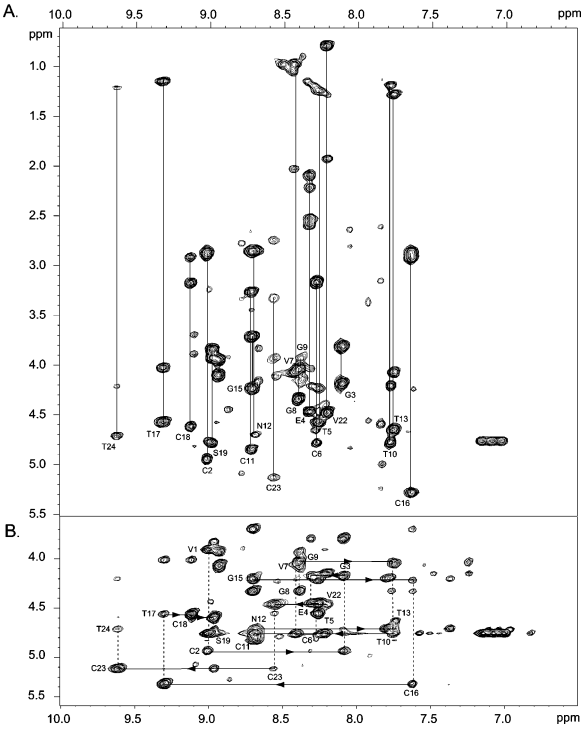

FIGURE 3: Two-dimensional ^{1}H NMR spectra of des-(24−28)-kalata B1. (A) The 750 MHz TOCSY spectrum of des-(24−28)-kalata B1 at 295 K in a 90% H_2O/10% ^2H_2O mixture at pH 4.0. Each spin system of the peptide was identified using standard protocols and is labeled accordingly. The resonances for Trp20 are absent from this display but were observed at other temperatures. (B) Fingerprint region of the 750 MHz NOESY spectrum of des-(24−28)-kalata B1 at 295 K in a 90% H_2O/10% ^2H_2O mixture at pH 4.0. The sequential connectivity pattern is broken only at the proline residues and Trp20.

^{1}H NMR Resonance Assignments. The peaks in the amide region of the two-dimensional total correlation spectroscopy (TOCSY) spectrum were well-dispersed, and the individual amino acid spin systems were readily identified, as illustrated in Figure 3. These were assigned to specific amino acid residues in the sequence using two-dimensional NOE spectroscopy (NOESY) experiments (*29*).

The fingerprint region of the NOESY spectrum (Figure 3) shows a complete cycle of αH−NH sequential connectivities for the whole protein, unbroken except at the proline residues and Trp20, whose signals were identified in other

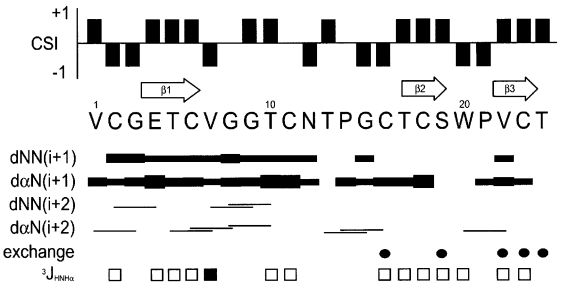

FIGURE 4: Summary of the sequential and medium-range NOE connectivities for des-(24−28)-kalata B1. The chemical shift index (CSI) of des-(24−28)-kalata B1 is shown as a bar plot, with values of ±1 indicating a shift deviation from random coil values of >0.1 ppm. Short-range NOEs are shown beneath the sequence. The thickness of the filled bars indicates NOE intensities. Slowly exchanging backbone amide protons with a $t_{1/2}$ of >20 h are indicated with filled circles. The $^3J_{HN-H\alpha}$ coupling constants above 8 Hz are shown as empty squares, and those below are shown as filled squares. The position of the β-strands deduced from the structures is shown above the sequence.

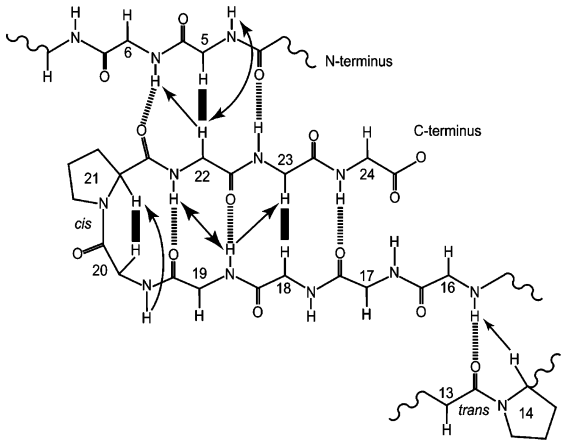

FIGURE 5: Schematic diagram of the secondary structure of des-(24−28)-kalata B1 showing the interstrand NOEs (solid arrows) and potential hydrogen bonds (dashed lines). Inter-residue HN−HN NOEs are shown with double-headed arrows; inter-residue Hα−HN NOEs are shown with single-headed arrows, and Hα−Hα NOEs are shown with thick lines. The peptide bonds between the proline residues and their preceding residues are denoted as either *cis* or *trans*. The α-carbon atoms are labeled according to their residue numbers. For clarity, sequential NOEs are omitted. The hydrogen bonds were inferred from slow exchange data and preliminary structure calculations.

spectra. The presence of $d_{\alpha(i-1)\rightarrow\delta(i)}$ NOEs and the absence of $d_{\alpha(i-1)-\alpha(i)}$ NOEs for Pro14 definitively confirmed that its preceding peptide bond is in a *trans* conformation. Pro21, however, was determined to be in the *cis* conformation by the $d_{\alpha(i)\rightarrow\alpha(i+1)}$ cross-peaks in the ^2H_2O NOESY spectrum (*14*). It is not uncommon for *cis*-proline residues to be present in constrained peptides, and there is a marked tendency for an aromatic amino acid (Tyr, Phe, or Trp) to favor the *cis* conformation (*30*).

Secondary Structure. Trends in chemical shifts provided a useful first insight into the structure of des-(24−28)-kalata B1. Chemical shift indices [CSI (*31*)] for the backbone α-protons were calculated using measured chemical shifts and published random coil values (*32*). A large proportion of the residues have shifts that differ from the random coil values by more than 0.1 ppm and hence have CSI values of ±1, suggesting that des-(24−28)-kalata B1 has a well-defined structure (Figure 4). The α-protons of Val7 and Ser19 had particularly large differences between their shifts and random coil chemical shifts. These residues lie on the turn regions of loops 2 and 5, respectively, and their chemical shifts are affected by the ring current effect of Trp20 in loop 5. Residues 4−6, 17−19, and 22−24 have positive CSI values, indicative of an extended structure. There are no stretches of more than three negative CSI values, which indicates that, like kalata B1, des-(24−28)-kalata B1 does not contain any helical regions. The remainder of the peptide displays an irregular pattern of alternating positive and negative CSI values, suggesting the presence of turns. This is further seen from the pattern of sequential NOEs. The $d_{\alpha N(i,i+2)}$ NOEs indicate the presence of turns in several regions of the peptide.

A schematic illustration of the major secondary structural elements of des-(24−28)-kalata B1 (Figure 5) was derived from consideration of the NOE, slow exchange, and coupling patterns of Figure 4. The secondary structure is similar to that of kalata B1, but is likely to be less compact or more flexible, evidenced by a reduction in the number of noncovalent contacts between backbone segments of des-(24−28)-kalata B1 relative to those in the circular peptide. The major secondary structural elements are the antiparallel β-strands (residues 17−19 and 22−24) linked by a β-hairpin. As for kalata B1, the turn in the hairpin centers around residues 20 and 21, as suggested by the negative CSI values and the presence of $d_{\alpha N(i,i+2)}$ NOEs. The extended regions of the hairpin, forming the β-strands, were identified by consideration of the positive CSI values, the slowly exchanging amide protons (which provide an indication of protection from the solvent associated with possible hydrogen bonding), and the large coupling constants.

The six cysteine residues in kalata B1 were originally predicted to form a I−IV, II−V, III−VI pattern of connectivity in preference to the other 14 possibilities (*4*). A recent study suggested an alternative disulfide bonding pattern (I−VI, II−V, III−IV) for native kalata B1 based on an alternative interpretation of 750 MHz NMR data (*33*). While we believe that this alternative is unlikely as it would not account for the exceptional stability of kalata B1, extra caution was taken during assignment of the disulfide connectivity of des-(24−28)-kalata B1. In particular, dihedral angle information proved to be valuable for discriminating between alternative possible disulfide connectivities. The side chain dihedral angles χ_1 for the Cys residues were determined by combining $^3J_{H\alpha H\beta}$ coupling constants from ECOSY spectra and interproton HN−Hα distances determined from NOESY spectra. From these results, together with the structure calculations described below, the disulfide connectivity of des-(24−28)-kalata B1 was determined to be Cys2−Cys16, Cys6−Cys18, Cys11−Cys23, i.e., I−IV, II−V, III−VI, as for the original assignment in native kalata B1. A recent report on the high-resolution structure of kalata B1 using similar methods has re-affirmed this disulfide bond connectivity (*34*).

Structure Determination. Solution structures were determined for des-(24−28)-kalata B1 by simulated annealing, including experimental distance restraints and dihedral angle restraints, with refinement by the explicit inclusion of water as a solvent. Of the final 50 calculated structures, the 20 lowest-energy structures consistent with experimental data

Table 1: Geometric and Energetic Statistics for Des-(24−28)-kalata B1[a]

energy (kcal/mol)	
overall	−605 ± 22
bond	7.48 ± 0.49
angle	45.6 ± 3.9
improper	12.76 ± 0.9
van der Waals	16.8 ± 1.2
cDih	0.257 ± 0.157
dihedral	91.5 ± 6.5
electrostatic	−803 ± 14
rmsd (Å)	
bonds	0.004 ± 0.0001
angles	0.75 ± 0.042
impropers	0.76 ± 0.04
NOEs	0.031 ± 0.003
cDih	0.06 ± 0.07
pairwise rmsd (Å)	
backbone atoms	0.57 ± 0.15
heavy atoms	0.90 ± 0.16
experimental data	
distance restraints	335
dihedral restraints	25
NOE violations of ≥0.20 Å	0
cdihedral violations of ≥2.0°	0
Ramachandran statistics (%)	
most favored	74
additionally allowed	26

[a] The values are given as means ± standard deviations for the ensemble of the 20 final solution structures.

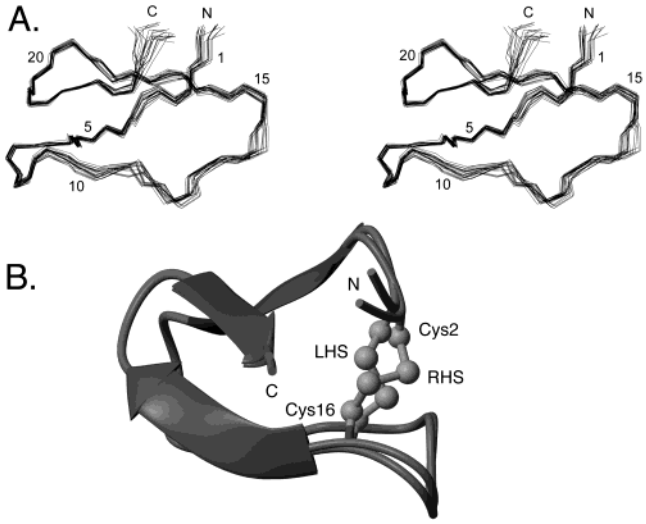

FIGURE 6: Structural features of the solution structure of des-(24−28)-kalata B1. (A) Stereoscopic representation of the solution structure of des-(24−28)-kalata B1. The 20 lowest-energy solution structures of des-(24−28)-kalata B1 are superimposed over the backbone atoms (N, C^{α}, and C^{o}). (B) Ribbon diagram of two representatives of the Cys2−Cys16 disulfide bond conformation of des-(24−28)-kalata B1. The Cys2−Cys16 disulfide bond (ball and stick) conformations are labeled as LHS (left-handed spiral) and RHS (right-handed spiral), as classified by the program PROMOTIF (*27*).

were chosen to represent the family of des-(24−28)-kalata B1 solution structures. A summary of the statistics for this family is given in Table 1. The structures are in agreement with the experimental data, with no distance violation exceeding 0.2 Å and no dihedral angle violation exceeding 2°. The des-(24−28)-kalata B1 solution structure is highly precise, as reflected in the backbone superposition of the final 20 structures in Figure 6A. Excellent structural convergence also extended to the majority of the side chains (excluding the terminal residues), providing detailed structural information for the positioning of side chains.

An analysis of the family of structures using the program PROMOTIF shows that the main element of secondary structure of des-(24−28)-kalata B1 is an antiparallel β-sheet, consistent with the prediction from the NMR chemical shift, coupling, and NOE data. Strand 1 (residues 17−19) and strand 2 (residues 22−24) are joined by a β-turn, forming a β-hairpin motif. A third β-strand, incorporating residues 4−6, is loosely associated with strand 2 but is not formally recognized as part of the β-sheet by PROMOTIF. A series of well-ordered turns accompany the β-sheet structure. In the view shown in Figure 6A, a type I β-turn comprising residues 6−9 lies directly beneath the type VIa1 turn involved in the β-hairpin. The latter turn type over residues 19−22 is consistent with the presence of a *cis*-Pro at position 3 of the turn (Figure 5). A type II turn is formed by residues 13−16 within the least well-defined loop, i.e., loop 3. These β-strand and tight turn structural elements are surrounded by a stable network of hydrogen bonds and hydrophobic interactions and, together with the knotted arrangement of disulfide bonds, account for the high level of definition of this acyclic permutant of kalata B1.

As is apparent from Figure 6A, the general fold of des-(24−28)-kalata B1 strongly resembles that of native kalata B1 (*4*), but with loop 6 excised from the structure. However, the breaking of the backbone introduces a subtle topological difference between the two forms, in terms of the type of cystine knot motif. The linear form fits into the inhibitor cystine knot (ICK) classification, while the cyclic form fits the cyclic cystine knot (CCK) classification (*15*). Associated with this appear to be some changes in disulfide bond flexibility in the acyclic form relative to native kalata B1. In des-(24−28)-kalata B1, the Cys6−Cys18 and Cys11−Cys23 disulfide bonds adopt a single type of conformation each, i.e., right-handed spiral and left-handed spiral, respectively. However, the Cys2−Cys16 disulfide bond adopts two possible conformations, shown in Figure 6B. In the family of 20 lowest-energy structures, this disulfide bond adopts a left-handed spiral conformation in 70% of the structures and a right-handed spiral in the remaining structures. These two disulfide bond conformations have similar χ_1 dihedral angles, consistent with the $J_{\alpha H\beta H}$ couplings measured in the ECOSY spectrum, but have different χ_2 and χ_3 angles. As there were no significant NOE restraint violations associated with either conformation, the NOE data are equally consistent with either conformation, or averaging between them, thus providing support for the proposal that there is greater flexibility in the acyclic permutant than in the native peptide. We cannot rule out the possibility that the increased structural disorder of the Cys2−Cys16 disulfide bond is due to a smaller total number of NOEs arising simply as a result of excision of loop 6. However, the fact that there is an equal number (21 nonsequential) of NOEs between the Hβ protons of Cys2 and Cys16 and other residues in kalata B1 and des-(24−28)-kalata B1 argues against this explanation and supports the idea that there is increased flexibility in the acyclic permutant. This is further supported by averaging of chemical shifts for the Hβ protons of Cys2 and Cys16, as described in more detail in the Discussion.

Biological Activity. It has been proposed that the various activities reported for cyclotides may be related to membrane disruption. A hemolytic assay was therefore considered a useful method for assessing the biological effects of acyclic

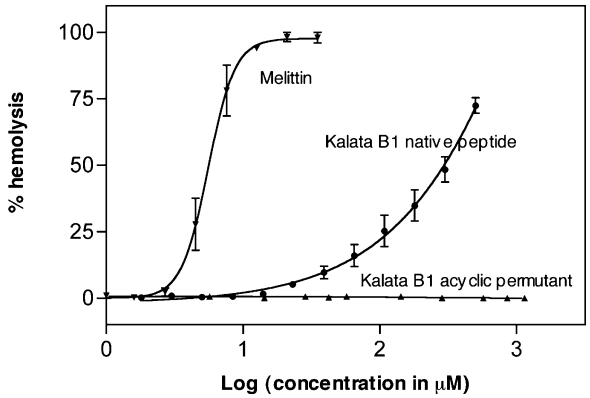

FIGURE 7: Percent hemolysis as a function of the log(peptide concentration). Error bars show the standard error of the mean. Fitted dose−response curves were generated using Graphpad Prism. The hemolytic activities were determined at peptide concentrations ranging from 1.8 to 500 μM for kalata B1, from 0.6 to 1140 μM for the acyclic permutant (in the C-terminal acid form), and from 0.6 to 35 μM for melittin.

permutation. Kalata B1 has been noted to have hemolytic activity (*10*, *35*); however, due to variations in the potencies reported previously, we have undertaken a thorough analysis of the potency of kalata B1 and des-(24−28)-kalata B1. Under a standard set of assay conditions, our results show that native kalata B1 induces 50% hemolysis (HD_{50}) at approximately 300 μM (Figure 7). This is intermediate between previously reported values, but the results are readily rationalized by noting that multiple factors, including the type, storage conditions, and incubation time of the red blood cells (RBCs), can significantly affect the results. It is important that any hemolytic assay is reported relative to a known standard, and in the study presented here, we found that the highly hemolytic bee venom peptide melittin had an HD_{50} of 5 μM, under the standard assay conditions (freshly isolated human RBCs, incubation for 1 h at room temperature with the peptide of interest), consistent with a wide range of literature data. Our previous value of 50 μM for kalata B1 (*35*) was obtained using RBCs from stored blood. Consistent with this lower value, in the current study we found that RBC storage for 3 days reduced the apparent HD_{50} value to <100 μM. Similarly, reducing the incubation time increased the apparent HD_{50}, most likely accounting for the higher value reported by Tam and co-workers for kalata B1 (*10*). Irrespective of the exact value, it can unequivocally be stated that kalata B1 has only mild hemolytic activity relative to melittin.

Truncating loop 6 of kalata B1 to produce des-(24−28)-kalata B1 not only removes five residues but also introduces N- and C-termini not present in the parent molecule. Previous studies showed no hemolytic activity of des-(24−28)-kalata B1 with an amidated C-terminus (*14*). In the current study, we have examined the influence of a negatively charged group by determining the hemolytic activity of des-(24−28)-kalata B1 containing a C-terminal acid. No hemolytic activity was observed up to a concentration of 1.2 mM (Figure 7). Thus, the mild hemolytic activity of kalata B1 is completely abolished by linearization of the peptide in loop 6.

DISCUSSION

In this study, we have synthesized an acyclic derivative of the prototypic cyclotide kalata B1 and determined its three-

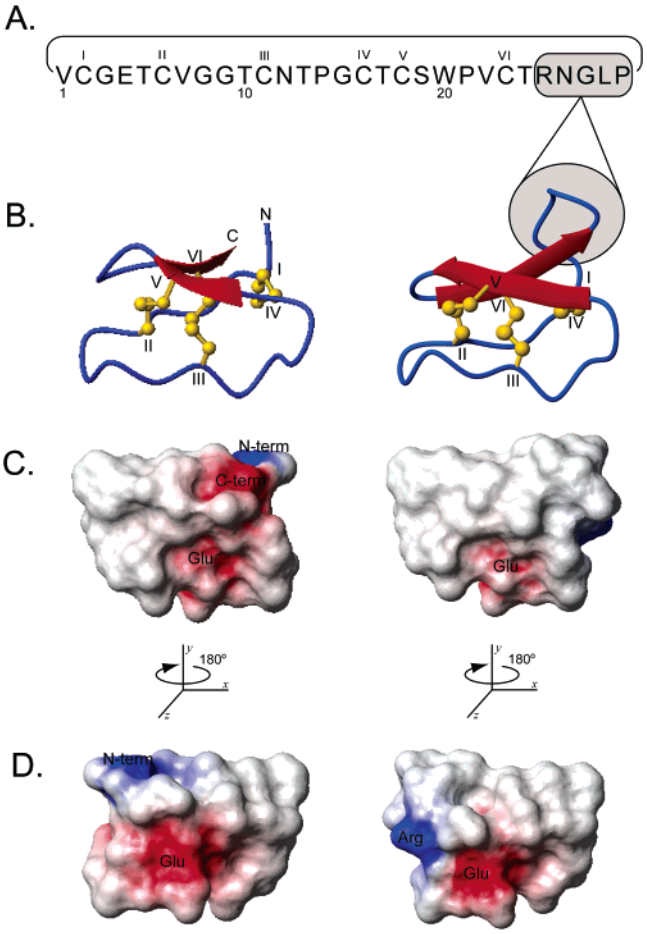

FIGURE 8: Structural comparison of the acyclic permutant des-(24−28)-kalata B1 and the native peptide kalata B1. (A) Amino acid sequence of des-(24−28)-kalata B1 with residues excised from native kalata B1 circled and shaded. (B) Ribbon diagrams of des-(24−28)-kalata B1 (left) and kalata B1 (right). Disulfide bonds are indicated with the contributing cysteine residues labeled I−VI according to their order in the amino acid sequence, as are the β-strands (arrows). Amino acid residues excised from kalata B1 to form des-(24−28)-kalata B1 are indicated in the kalata B1 ribbon diagram (right). (C and D) Electrostatic potential surface diagrams of des-(24−28)-kalata B1 (left) and kalata B1 (right), rotated 180° about the *y*-axis. Residues that contribute to the electrostatic potential surface are labeled.

dimensional structure. Breaking the backbone in loop 6 of the cyclotide structure is shown not to have a major effect on the three-dimensional fold, but has a dramatic effect on hemolytic activity. A previous study (*14*) of kalata B1 and its acyclic permutants reported the loss of hemolytic activity with linearization of the peptide backbone, but structural characterization of various acyclic permutants was limited to a chemical shift analysis. We show here that although the overall structure remains intact, removal of residues 24−28 of kalata B1 causes disruption of some structural features that are important to overall stability, and in particular introduces some flexibility into the Cys2−Cys16 disulfide bond.

Figure 8 shows a comparison of the structural features of native kalata B1 and the acyclic permutant, des-(24−28)-kalata B1, studied here. Panel A shows the region of the peptide sequence that has been excised, and panel B shows that this excision makes a minimal difference in the overall fold of the peptide and maintains the β-hairpin, tight turns, and cystine knot connectivity of the native peptide.

While the overall fold remains unchanged, a detailed analysis of the des-(24−28)-kalata B1 structure shows that there are some differences associated with the side chains. In particular, the Cys2−Cys16 disulfide bond forms a left-handed spiral conformation in 14 of the 20 lowest-energy structures and a right-handed spiral in the remaining six structures. In contrast, this same disulfide bond forms exclusively a left-handed spiral conformation in cyclic native kalata B1. This change appears to be caused not by a smaller number of local NOE restraints in the acyclic permutant but rather by increased flexibility because it is associated with a marked reduction in the separation of β-proton chemical shifts for Cys2 and Cys16. For example, the Hβ shift separation of 1.2 ppm for Cys16 in kalata B1 is reduced to 0.07 ppm in des-(24−28)-kalata B1. The cyclic peptide backbone of kalata B1 may contribute to the stability of the molecule by favoring a single conformation for this disulfide bond.

Further analysis of the des-(24−28)-kalata B1 family of structures shows that Glu4 adopts two orientations, as opposed to a single well-defined orientation in kalata B1. In the major conformation in the calculated structures, Glu4 forms a hydrogen bond with the backbone NH group of Asn12, which is consistent with recent high-resolution structures of kalata B1 (*34*). The alternative Glu4 conformation orients the side chain in another direction, inconsistent with the presence of a Glu4−Asn12 hydrogen bond. As a pH of 4, close to the pK_a of glutamic acid, was used in the structural study of des-(24−28)-kalata B1, the side chain of Glu4 may exist in both charged and neutral forms, explaining the presence of two conformations for Glu4. The conformational interchange must be fast on the chemical shift time scale, as no evidence of multiple sets of peaks was observed in the spectra. The apparent structural flexibility in des-(24−28)-kalata B1 is supported by the increase in amide exchange rates relative to that of native kalata B1, suggesting a generally more flexible or less stable conformation (*14*).

A comparison of the solvent accessible surfaces of des-(24−28)-kalata B1 and native kalata B1 shown in Figure 8 (C and D) allows other similarities and differences to be identified. Both are flattened spherical molecules with no large pockets or protuberances, but the N-terminus of des-(24−28)-kalata B1 protrudes slightly and provides a local point of difference between the two molecules. Only the anionic Glu4 and cationic N-terminus contribute to the electrostatic potential surface of des-(24−28)-kalata B1, with the majority of the surface-exposed residues being hydrophobic in nature. The electrostatic potential surface of native kalata B1 is similar to that of des-(24−28)-kalata B1, as the positively charged Arg25 residue effectively replaces the charge at the N-terminus lost on cyclization (Figure 8D).

In this study, we have remeasured the hemolytic activity of kalata B1 because of the variation observed in previous results, which range from approximately 50 to 1500 μM (*10*, *35*). We have confirmed that kalata B1 does have mild hemolytic activity, with an HD_{50} value intermediate between the previous results, and that the apparent activity is sensitive to experimental variables that include the storage age of the blood used and the incubation time in the assay. We have further shown that hemolytic activity is completely abolished by breaking the peptide backbone in loop 6, and introducing either a charged or an amidated C-terminus. Thus, electrostatic factors associated with the introduced termini do not appear to be primarily responsible for the loss of hemolytic activity in acyclic derivatives. The electrostatic surface potentials in Figure 8 show that both cyclic and acyclic forms have a single positive and single negative charge on one face of the molecule, albeit in slightly different relative locations.

The overall shapes of des-(24−28)-kalata B1 with kalata B1 are similar and hence cannot explain the difference in hemolytic activity, unless the residues excised from the native peptide are directly involved in hemolytic activity. As neither the shape nor charge distribution of the molecules is sufficiently different to explain the differences in hemolytic activity, it may be that differences in the dynamic stability of the molecules are important. The NMR data show that cyclization stabilizes the Cys2−Cys16 disulfide bond conformation and provides a general tightening of the molecule. Further mutagenesis and dynamics studies are necessary to confirm this suggestion.

The acyclic derivative studied here is of particular interest as the break in the backbone is located in a region of the molecule that may play an important role in the biosynthesis of the circular backbone of the cyclotides. The gene sequence of kalata B1 (*3*) suggests that the peptide is produced via post-translational processing from a precursor protein, with cyclization occurring in loop 6. It is currently not known whether cyclization occurs after or before disulfide bond formation, but the fact that the acyclic molecule folds into a three-dimensional structure so similar to the native form is consistent with cyclization occurring after folding and formation of the disulfide bonds.

Des-(24−28)-kalata B1 is also of interest because it is topologically equivalent to numerous linear cystine knot-containing peptides from a wide range of organisms. Support for the idea that cyclization of kalata B1 occurs after disulfide formation comes from the fact that many of the other naturally occurring acyclic cystine knot proteins occur in plants, including, for example, the squash trypsin inhibitors (*36*, *37*). Interestingly, naturally occurring cyclic squash trypsin inhibitors (MCoTIs) have recently been found in the seeds of *Momordica cochinchinensis* (*38*). The structure of one of these peptides, MCoTI-II, has been determined by NMR spectroscopy (*39*, *40*) and reveals a cyclic cystine knot motif. Although the only sequence conservation between the MCoTI peptides and the cyclotides includes the six cysteine residues, the structural similarity suggests that they are evolutionarily related (*39*). To date, no naturally occurring linear analogues of cyclotides from the Rubiaceae and Violaceae families have been found. However, the study presented here confirms that a well-defined structure, with a topology equivalent to that of linear cystine knot proteins, is possible despite there being no known examples discovered so far.

The structure of MCoTI-II is similar to acyclic squash peptides but displays significant disorder in loop 6. Thus, cyclization does not necessarily lead to a more well-defined structure in all cases. In the case of MCoTI-II, it has been suggested that cyclization may have evolved to reduce susceptibility to attack by proteases (*39*). This may also be a driving force for cyclization of kalata B1, but in this study, we have shown that for kalata B1 there also appears to be definite stabilization of one of the disulfide bonds as a result of backbone cyclization. Cyclization may have dual roles

of limiting proteolytic cleavage and enhancing structural homogeneity.

In conclusion, the three-dimensional structure of des-(24−28)-kalata B1 retains the major structural features of native kalata B1, suggesting that the cyclic backbone is not critical in defining the overall fold. However, localized regions of the peptide, and in particular one of the disulfide bonds, are stabilized by cyclization. It appears that the loss of hemolytic activity associated with breaking the cyclic backbone is due to a loss of structural stability.

REFERENCES

1. Craik, D. J., Daly, N. L., Bond, T., and Waine, C. (1999) *J. Mol. Biol. 294*, 1327−1336.
2. Craik, D. J., Simonsen, S., and Daly, N. L. (2002) *Curr. Opin. Drug Discovery Dev. 5*, 251−260.
3. Jennings, C., West, J., Waine, C., Craik, D., and Anderson, M. (2001) *Proc. Natl. Acad. Sci. U.S.A. 98*, 10614−10619.
4. Saether, O., Craik, D. J., Campbell, I. D., Sletten, K., Juul, J., and Norman, D. G. (1995) *Biochemistry 34*, 4147−4158.
5. Trabi, M., and Craik, D. J. (2002) *Trends Biochem. Sci. 27*, 132−138.
6. Williams, N. K., Prosselkov, P., Liepinsh, E., Line, I., Sharipo, A., Littler, D. R., Curmi, P. M., Otting, G., and Dixon, N. E. (2002) *J. Biol. Chem. 277*, 7790−7798.
7. Deechongkit, S., and Kelly, J. W. (2002) *J. Am. Chem. Soc. 124*, 4980−4986.
8. Iwai, H., and Pluckthun, A. (1999) *FEBS Lett. 459*, 166−172.
9. Gustafson, K. R., Sowder, R. C., II, Henderson, L. E., Parsons, I. C., Kashman, Y., Cardellina, J. H., II, McMahon, J. B., Buckheit, R. W., Jr., Pannell, L. K., and Boyd, M. R. (1994) *J. Am. Chem. Soc. 116*, 9337−9338.
10. Tam, J. P., Lu, Y. A., Yang, J. L., and Chiu, K. W. (1999) *Proc. Natl. Acad. Sci. U.S.A. 96*, 8913−8918.
11. Witherup, K. M., Bogusky, M. J., Anderson, P. S., Ramjit, H., Ransom, R. W., Wood, T., and Sardana, M. (1994) *J. Nat. Prod. 57*, 1619−1625.
12. Lindholm, P. U. G. S. J., Claeson, P., Gulbo, J., Larsson, R., Bohlin, L., and Backlund, A. (2002) *Mol. Cancer Ther. 1*, 365−369.
13. Schöpke, T., Hasan Agha, M. I., Kraft, R., Otto, A., and Hiller, K. (1993) *Sci. Pharm. 61*, 145−153.
14. Daly, N. L., and Craik, D. J. (2000) *J. Biol. Chem. 275*, 19068−19075.
15. Craik, D. J., Daly, N. L., and Waine, C. (2001) *Toxicon 39*, 43−60.
16. Marion, D., and Wüthrich, K. (1983) *Biochem. Biophys. Res. Commun. 113*, 967−974.
17. Rance, M., Sørensen, O. W., Bodenhausen, G., Wagner, G., Ernst, R. R., and Wüthrich, K. (1983) *Biochem. Biophys. Res. Commun. 117*, 479−485.
18. Braunschweiler, L., and Ernst, R. R. (1983) *J. Magn. Reson. 53*, 521−528.
19. Bax, A., and Davis, D. G. (1985) *J. Magn. Reson. 65*, 355−360.
20. Griesinger, C., Sørensen, O. W., and Ernst, R. R. (1987) *J. Magn. Reson. 75*, 474−492.
21. Jeener, J., Meier, B. H., Bachmann, P., and Ernst, R. R. (1979) *J. Chem. Phys. 71*, 4546−4553.
22. Piotto, M., Saudek, V., and Sklenar, V. (1992) *J. Biomol. NMR 2*, 661−665.
23. Eccles, C., Guntert, P., Billeter, M., and Wüthrich, K. (1991) *J. Biomol. NMR 1*, 111−130.
24. Guntert, P., Mumenthaler, C., and Wüthrich, K. (1997) *J. Mol. Biol. 273*, 283−298.
25. Brünger, A. T., Adams, P. D., and Rice, L. M. (1997) *Structure 5*, 325−336.
26. Linge, J. P., and Nilges, M. (1999) *J. Biomol. NMR 13*, 51−59.
27. Hutchinson, E. G., and Thornton, J. M. (1996) *Protein Sci. 5*, 212−220.
28. Laskowski, R. A., Rullmannn, J. A., MacArthur, M. W., Kaptein, R., and Thornton, J. M. (1996) *J. Biomol. NMR 8*, 477−486.
29. Wüthrich, K. (1986) *NMR of Proteins and Nucleic Acids*, Wiley-Interscience, New York.
30. Wu, W. J., and Raleigh, D. P. (1998) *Biopolymers 45*, 381−394.
31. Wishart, D. S., Sykes, B. D., and Richards, F. M. (1992) *Biochemistry 31*, 1647−1651.
32. Merutka, G., Dyson, H. J., and Wright, P. E. (1995) *J. Biomol. NMR 5*, 14−24.
33. Skjeldal, L., Gran, L., Sletten, K., and Volkman, B. F. (2002) *Arch. Biochem. Biophys. 399*, 142−148.
34. Rosengren, K. J., Daly, N. L., Plan, M. R., Waine, C., and Craik, D. J. (2003) *J. Biol. Chem. 278*, 8606−8616.
35. Daly, N. L., Love, S., Alewood, P. F., and Craik, D. J. (1999) *Biochemistry 38*, 10606−10614.
36. Holak, T. A., Gondol, D., Otlewski, J., and Wilusz, T. (1989) *J. Mol. Biol. 210*, 635−648.
37. Helland, R., Berglund, G. I., Otlewski, J., Apostoluk, W., Andersen, O. A., Willassen, N. P., and Smalas, A. O. (1999) *Acta Crystallogr. D55*, 139−148.
38. Hernandez, J. F., Gagnon, J., Chiche, L., Nguyen, T. M., Andrieu, J. P., Heitz, A., Trinh Hong, T., Pham, T. T., and Le Nguyen, D. (2000) *Biochemistry 39*, 5722−5730.
39. Felizmenio-Quimio, M. E., Daly, N. L., and Craik, D. J. (2001) *J. Biol. Chem. 276*, 22875−22882.
40. Heitz, A., Hernandez, J. F., Gagnon, J., Hong, T. T., Pham, T. T., Nguyen, T. M., Le-Nguyen, D., and Chiche, L. (2001) *Biochemistry 40*, 7973−7983.

BI027323N